P.O.Box 2345, Beijing 100023,China
Fax: +86-10-85381893
E-mail: wjg@wjgnet.com www.wjgnet.com

World J Gastroenterol 2004;10(1):67-72
World Journal of Gastroenterology
 ISSN 1007-9327

• LIVER CANCER •

Single-level dynamic spiral CT of hepatocellular carcinoma: Correlation between imaging features and density of tumor microvessels

Wei-Xia Chen, Peng-Qiu Min, Bin Song, Bong-Liang Xiao, Yan Liu, Ying-Hui Ge

Wei-Xia Chen, Peng-Qiu Min, Bin Song, Department of Radiology, West China Hospital, Sichuan University, Chengdu 610041, Sichuan Province, China
Bong-Liang Xiao, Department of Toxicology and Pathology, School of Public Health, Sichuan University, Chengdu 610041, Sichuan Province, China
Yan Liu, Department of Radiology, West China Hospital, Sichuan University, now working in Rijin Hospital, Shanghai, China
Ying-Hui Ge, Department of Radiology, West China Hospital, Sichuan University, now working in Henan Province Hospital, Henan Province, China
Correspondence to: Wei-Xia Chen, MD, Department of Radiology, West China Hospital, Sichuan University, Chengdu 610041, Sichuan Province, China. wxchen25@sohu.com
Telephone: +86-28-85422595 **Fax:** +86-28-85582944
Received: 2003-06-21 **Accepted:** 2003-07-30

Abstract

AIM: To investigate the correlation of enhancement features of hepatocellular carcinoma (HCC) revealed by single-level dynamic spiral CT scanning (DSCT) with tumor microvessel density (MVD), and to determine the validity of DSCT in assessing *in vivo* tumor angiogenic activity of HCC.

METHODS: Twenty six HCC patients were diagnosed histopathologically. DSCT was performed for all patients according to standard scanning protocol. Time-density curves were generated, relevant curve parameters were measured, and gross enhancement morphology was analyzed. Operation was performed to remove HCC lesions 1 to 2 weeks following CT scan. Histopathological slides were carefully prepared for the standard F_8RA immunohistochemical staining and tumor microvessel counting. Enhancement imaging features of HCC lesions were correlatively studied with tumor MVD and its intra-tumor distribution characteristics.

RESULTS: On DSCT images of HCC lesions, three patterns of time-density curve and three types of gross enhancement morphology were recognized. Histomorphologically, the distribution of positively stained tumor endothelial cells within tumor was categorized into 3 types. Curve parameters such as peak enhancement value and contrast enhancement ratio were significantly correlated with tumor tissue MVD (r=0.508 and r=0.423, P<0.01 and P<0.05 respectively). Both the pattern of time-density curve and the gross enhancement morphology of HCC lesions were also correlated with tumor MVD, and reflected the distributive features of tumor microvessels within HCC lesions. Correlation between the likelihood of intrahepatic metastasis of HCC lesions with densely enhanced pseudocapsules and rich pseudocapsular tumor MVD was found.

CONCLUSION: Enhancement imaging features of HCC lesions on DSCT scanning are correlated with tumor MVD, and reflect the intra-tumor distribution characteristics of tumor microvessels. DSCT is valuable in assessing the angiogenic activity and tumor neovascularity of HCC patients *in vivo*.

Chen WX, Min PQ, Song B, Xiao BL, Liu Y, Ge YH. Single-level dynamic spiral CT of hepatocellular carcinoma: Correlation between imaging features and density of tumor microvessels. *World J Gastroenterol* 2004; 10(1): 67-72
http://www.wjgnet.com/1007-9327/10/67.asp

INTRODUCTION

Tumor angiogenesis plays a fundamental role in the pathogenesis of tumor growth and metastasis[1-3], and significantly influences the biological behaviors of tumor and prognosis of patients[3-6]. The inhibition or blockade of this angiogenic activity, on the other hand, can slow down the tumor growth rate and positively affect the outcome of patients[7-9]. Although a single standardized and thoroughly validated method to evaluate the structure and function of tumor angiogenesis is not available, some histomorphological markers, such as microvessel density (MVD) and vascular endothelial growth factor, have been used as indicators of tumor angiogenic activity currently[3,10-12]. However, these markers were studied immunohistochemically *in vitro* on biopsy or surgical tissues, and could not provide information of functional status of tumor angiogenesis, and were hardly to repeat for patients in follow-up. An ideal test should be non-invasive, fast, easy to perform, repeatable and reproducible, and most importantly, it should provide accurate and comprehensive information on the structure and biological characteristics of tumors *in vivo*.

Modern medical imaging modalities can depict the blood flow or reflect the hemodynamic changes. Recent studies using Doppler Sonography[13-16] or MR[17-28] or CT[29,30] to assess tumor angiogenesis and neovascularity have yielded encouraging results in differential diagnosis and the correlation of aggressiveness and metastasis of tumor with the prognosis of patients. Correlation of enhanced imaging features of hepatocellular carcinoma (HCC) with tumor MVD was investigated to determine the validity of single-level dynamic spiral CT scanning (DSCT) *in vivo* for assessment of tumor angiogenic activity and neovascularity.

MATERIALS AND METHODS

Study subjects

From June 1997 to January 1999, 26 HCC patients were histopathologically proved and used for the study, and all the patients met the criteria for DSCT scanning and for histopathological specimen sampling and slides preparation. There were 23 males and 3 females with a mean age of 43.5 years (27 to 72 years). None of them had anti-tumor therapies prior to CT examination, and 1-2 weeks after CT, surgery was performed on all HCC patients to remove the lesions.

DSCT protocol

A Somatom Plus 4 VA spiral CT scanner (Siemens, Erlangen, Germany) was used for the study, 2 ml/kg of 65% angiografin or ultravist-300 (Schering, Germany) was used as intravenous contrast agent and injected via the antecubital route on the constant rate of 3 ml/sec. Before the start of CT scanning, the patients were educated and trained on how to cooperate for CT examination. The whole scanning procedure included 3 steps. First, all the liver was scanned without enhancement, then dynamic scanning at the selected target slice level (single-slice dynamic scanning) was followed, and finally the portal venous phase spiral CT acquisition of the entire liver was obtained. The target slice was selected based on the abnormal findings on the initial scanning. Only the central slice with the smallest area of tumor necrosis was chosen as the target for dynamic scanning. The dynamic scanning was performed 18 seconds after intravenous administration of contrast agent. For the dynamic scanning the sequence scan mode was employed with the cycle time of 2.3 seconds. A total of 18 slices were generated. The spiral scan mode was used for the initial scan and acquisition data on the final portal venous phase. Seven mm was used for calibration, table feed and slice thickness (pitch=1/1), and the scan delay time for the portal venous phase was 65 seconds.

Image data processing

Generation of time-density (T-D) curve Any visible blood vessel, necrotic foci and hypodense septum were avoided in selection of the region of interest (ROI) for HCC lesions. For the abdominal aorta, ROI was placed in its cross sectional center. The size of ROI was restricted to around 1 cm in diameter. With the built-in software program, the T-D curves of both HCC lesions and abdominal aorta were generated on the basis of the selected ROIs.

T-D curve parameters Several curve parameters were defined for the T-D curve of HCC lesions. (a) The peak enhancement value (PV) of the abdominal aorta was defined as the CT attenuation number at the junction between the up-slope portion with the steepest rise and the portion with gradual or flat rise. The corresponding time was referred to as the peak enhancement time (PT). (b) The PV for HCC lesion was the result of maximum enhancement CT attenuation number minus the baseline CT attenuation number on plain CT scan, and the time to reach the maximum CT attenuation number after enhancement was the PT. (c) The contrast enhancement ratio (CER) was defined as the percentage of the PV of HCC lesion divided by the PV of the abdominal aorta. Patterns of T-D curves were analyzed and the related curve parameters (PV, PT, and CER) were calculated.

Image interpretation All the CT images were jointly analyzed with standardized criteria by two senior radiologists experienced in liver imaging. Special attention was paid to the morphological enhancement patterns of HCC lesions and other associated imaging findings, such as pseudocapsules, daughter foci, and invasion of the portal venous system.

Histomorphological analysis of tissue specimen

Great care was taken to ensure that the matching of tissue sampling sites of surgically resected gross HCC tumor specimen with the correspondingly selected ROIs on DSCT images was on one-to-one basis. The obtained tissue specimens were processed by standard macro- and micro-slide techniques to verify the histomorphological tumor extension. Then slides of 5 μm thickness were stained with the standard immunoperoxidase method using factor VIII-related antigen (F_8RA stain)[2]. Criteria for positive stain and microvessel counting were those established by Weidner *et al*[2-3]. Two independent experienced pathologists counted each ROI separately, and consensus counting was done for dispute. The counting was first proceeded at 100 x magnification for "hot spot" representing the area of the highest microvessel density (MVD), then switched to 200 x magnification for clear depiction and better counting. For each slide three "hot spots" were counted, and the mean count represented the final MVD. The distribution of "hot spots" within tumor lesions was also recorded.

Statistical analysis

Pearson' s correlation analysis and variance analysis were performed to test the strength of association between CT imaging features and the histomorphological marker, $P<0.05$ was considered statistically significant.

RESULTS

Dynamic CT scan

Patterns of T-D curve Some distinctively different patterns of T-D curves of HCC lesions were observed and categorized into three types. Type I, the initial rise of T-D curve was very fast and steep, then abruptly changed to a more flat and steady gradual rise till the plateau phase. This curve pattern occurred in 7 patients. In type II curve, the up-rise of the curve slope was obvious, yet relatively smooth, no abrupt turn in the configuration of the curve up-slope. Thirteen patients demonstrated T-D curve pattern of type II. Type III curve in 6 patients was characterized by slow and flat rise of the initial curve up-slope with low amplitude. These three patterns of T-D curves of HCC lesions are depicted in Figure 1, and the calculated curve parameters are summarized in Table 1. PV and CER of type III patients were obviously lower than those of type I and type II patients, and the differences were statistically significant ($P<0.05$). On the other hand, the differences of PV and CER between type I and type II patients were not statistically significant. There was a trend for PT to increase gradually from type I to type III, but the differences among the three types were not statistically significant.

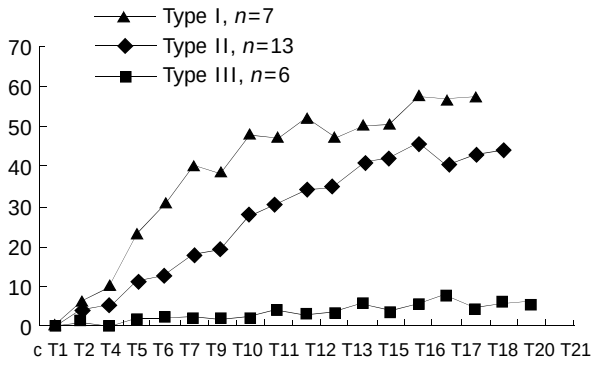

Figure 1 Three patterns (I, II, III) of time-density curve observed in HCC patients. The transverse axis represents the time and the Y-axis represents the peak enhancement value in Hounsfield units.

Table 1 HCC time-density curve patterns

Curve parameters	Type I	Type II	Type III
Number of patients	7	13	6
PV (Hu)	53.6±7.8	47.9±12.6	20.6±7.2[a]
PT (Sec)	43.8±9.5	52.2±7.7	57.9±8.3
CER (%)	25.0± 7.2	22.5±6.5	8.2±3.4[a]

[a]The differences of PV and CER between type III and those of type I and II were statistically significant ($P<0.05$).

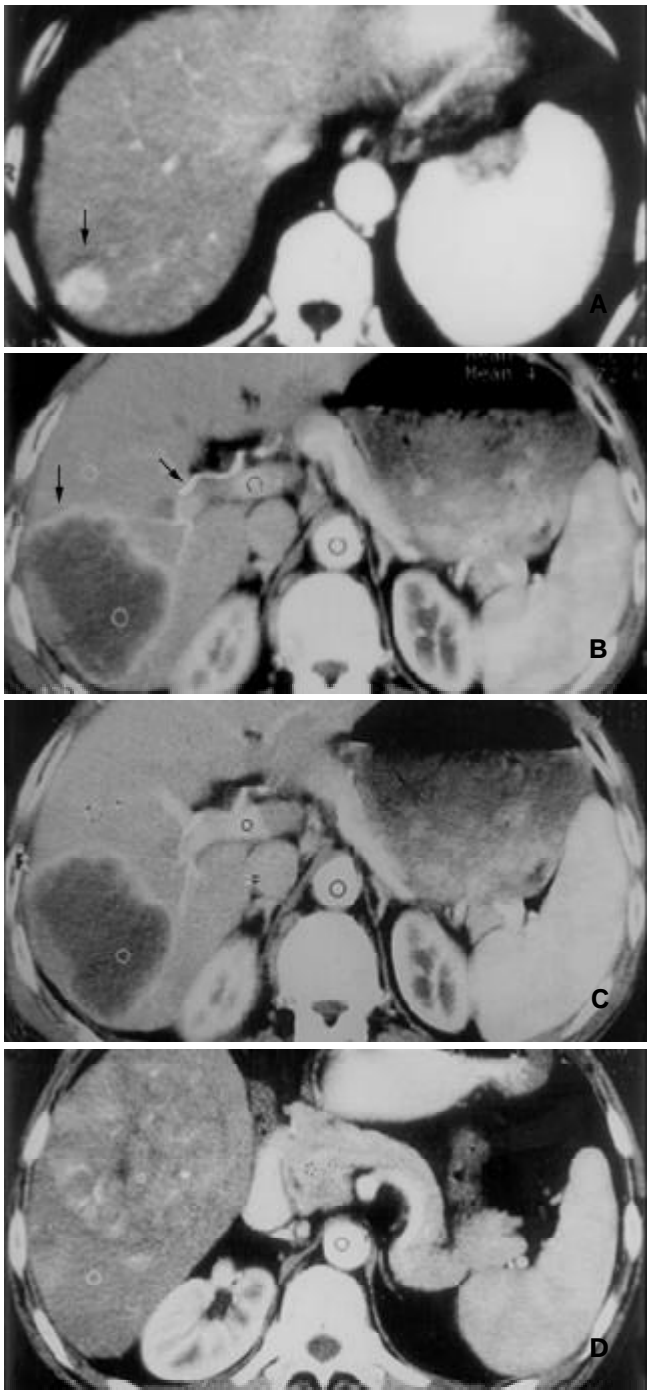

Figure 2 Three types of enhancement morphology depicted in HCC patients. A: Type A. Marked and homogeneous enhancement of the entire HCC lesion in the posterosuperior segment of right hepatic lobe (black arrow). B: Type B. Bright peripheral ring-like enhancement of HCC lesion on arterial phase image in the right posterosuperior segment (black arrow), and the dilated right hepatic artery (black arrow). C: Portal venous image at the same slice level as in (B). HCC lesion remained hypodense despite obvious enhancement of normal liver parenchyma elsewhere. D: Type C. Inhomogeneous patchy enhancement of HCC lesion in right lower hepatic lobe from arterial phase image. Bright dots and linear shadows represent enhanced tumor vessels within the lesion.

Morphological enhancement patterns of HCC The gross morphological enhancement manifestations of HCC lesions could also be grouped into 3 types (Figure 2). Type A was seen in 7 patients, the HCC lesions were densely enhanced in a homogeneous pattern (Figure 2A). The mean transverse diameter of lesions was 3.1 cm. Type B was in 5 patients, the lesions demonstrated complete or partial rim-like peripheral enhancement, without or with only few dots of enhanced tumor vessels within the lesion center (Figure 2B, 2C). Mean diameter was 5.7 cm. Type C was seen in 14 patients, HCC lesions were inhomogeneously enhanced in a patchy fashion. Many small round-shaped, linear or reticular shadows representing enhanced tumor vessels were clearly visible, along with many hypodense necrotic foci and fibrous septa within the lesions (Figure 2D). The mean transverse diameter in this group of patients was 8.5 cm. The differences in the transverse diameter of tumor lesions among the three groups were statistically significant.

Immunohistochemical findings

F_8RA staining revealed a great variation in the distribution of positively stained tumor vascular endothelial cells within HCC lesions. Such a distribution variability in our patient could be roughly grouped into three patterns (Figure 3). (1) Twelve patients exhibited very rich blood sinusoids but scanty tumor microvessels in the interstitium. In 9 patients, positively stained sinusoidal endothelial cells were abundant and distributed inhomogeneously in a patchy fashion (Figure 3A). But in the rest 3 patients, sinusoidal endothelial cells had no positive staining. (2) Eleven patients had both rich sinusoids and interstitial microvessels, a large number of positively stained endothelial cells were distributed in both sinusoids and interstitium (Figure 3B). (3) Three patients had rich interstitium, with few interstitial microvessels and scanty sinusoids, and positively stained endothelial cells were very scarce (Figure 3C).

The MVD of HCC tumor tissue varied greatly from 6 to 91 among patients.

Correlation of DSCT features and tumor MVD

(1) T-D curve parameters and MVD A statistically significant positive correlation was demonstrated between tumor MVD and both PV and CER of corresponding HCC lesions. The correlation coefficients (r) were 0.508 ($P<0.01$) and 0.423 ($P<0.05$) respectively. However, MVD had no positive correlation with PT.

(2) Curve patterns, enhancement morphology and MVD The relationships between tumor MVD and T-D curve patterns and the three gross enhancement morphological types of HCC lesions are summarized in Table 2. The tumor MVDs of T-D curve type III and the gross enhancement morphology type B were significantly lower than those of curve type I and II ($P<0.05$), and gross morphology type A and C ($P<0.05$), respectively. The differences of MVDs between types I, II of T-D curve and the enhancement morphological patterns (type A, C) were not statistically significant.

Table 2 HCC time-density curve patterns, types of gross enhancement morphology and tumor MVD

	Type I	Type II	Type III	Type A	Type B	Type C
Patient No	7	13	6	7	5	14
MVD	41.8±16.7	48.0±18.2	23.0±7.4[a]	49.7±14.2	15.6±5.7[b]	44.0±19.7

[a]The differences of MVDs between type III and type I, type II were statistically significant ($P<0.05$). [b]The differences of MVDs between types B, A, C were statistically significant ($P<0.05$).

(3) Curve patterns, enhancement morphology and distribution of MVD The intratumoral distribution characteristics of tumor MVD and their relationships with T-D curve patterns and gross morphological enhancement types of HCC lesions are listed in Table 3.

Table 3 HCC time-density curve patterns, types of gross enhancement morphology and intratumoral MVD distribution

	Type I	Type II	Type III	Type A	Type B	Type C
Rich S	0	10	2	4	2	6
Rich S & I MVD	7	3	1	3	0	8
Scanty S & I MVD	0	0	3	0	3	0

S-tumor blood sinusoids, I-tumor interstitium.

(4) Other DSCT signs and related histomorphological changes Eleven patients demonstrated intrahepatic metastatic foci or daughter lesions. 7 of the 11 patients had prominent pseudocapsules that were hyperdense on DSCT images (Figure 4). In 1 patient the pseudocapsule remained to be hypodense throughout the entire scanning period, and no discrete pseudocapsule was discernible in the other 3 patients. Immunohistochemical F_8RA stain revealed abundant positively stained tumor endothelial cells in connective tissue of the tumor pseudocapsule in 8 patients. In the remaining 3 patients, judgement could not be made as whether or not the tumor pseudocapsule was present on the histopathological slides, due to improper tissue sampling, which missed the border region between HCC lesion and the neighboring normal liver tissue.

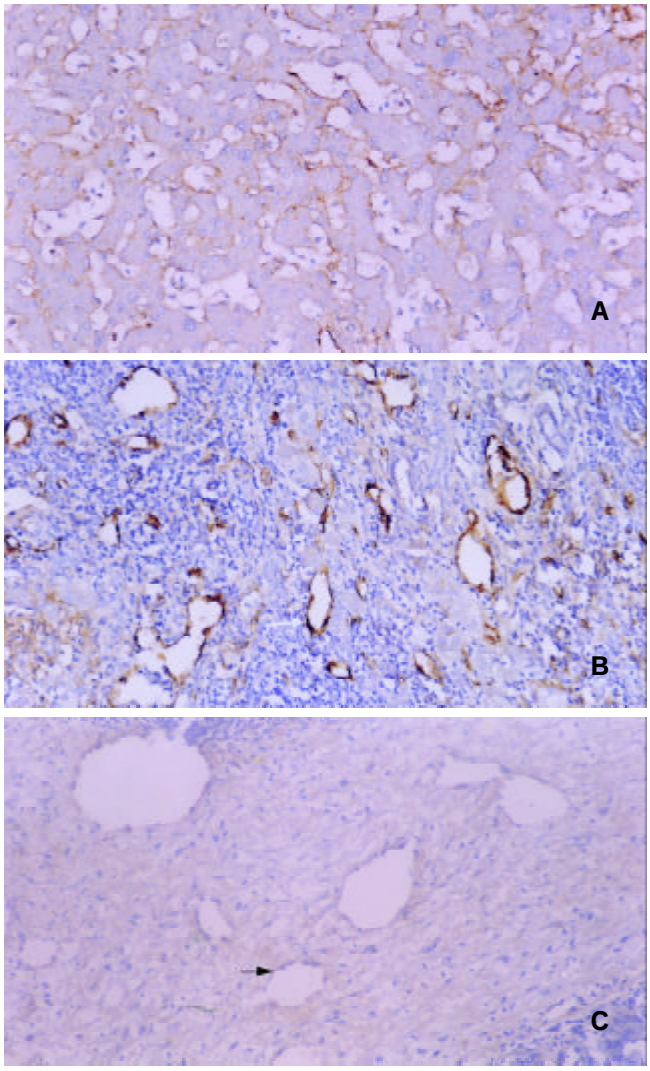

Figure 3 Three patterns of intratumoral MVD distribution revealed by F_8RA immunohistochemical staining. A: Pattern I. Markedly dilated and abundant blood sinusoids with very rich positively stained sinusoidal endothelial cells and scanty tumor interstitium. B: Pattern II. Sinusoids and interstitium abundant and rich in positively stained endothelial cells (black arrow). C: Pattern III. Rich tumor interstitium with few positively stained endothelial cells (white arrow) and scanty blood sinusoids.

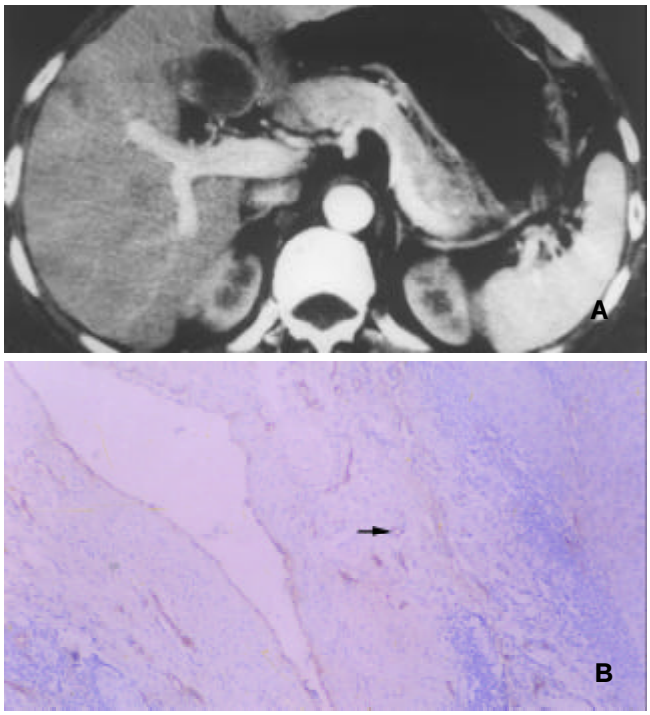

Figure 4 Enhancement of HCC pseudocapsules and pseudocapsular MVD. A: Marked enhancement of HCC pseudocapsule (hyperdensity) in the medial segment of left hepatic lobe shown by DSCT. Note the similar enhancement pattern of the satellite or daughter lesion in the anterior segment of right hepatic lobe. B: F_8RA staining Rich positively stained endothelial cells within tumor pseudocapsule (black arrow) revealed by F_8RA staining.

DISCUSSION

MVD, one of the histomorphological markers, is currently regarded as the best available means to represent tumor angiogenesis, and has been widely used to characterize tumor angiogenic activity *in vitro*. However, it may not be an ideal method for clinical purposes, as it is invasive and hard to perform and to repeat. Clearly, from the clinical perspective, it is of great clinical importance to look for a noninvasive method, which can provide *in vivo* overall functional information about tumor angiogenesis, besides accurate morphological information. We designed this dynamic spiral CT study to investigate the correlation of enhancement patterns of HCC lesions with the histomorphological marker of tumor angiogenesis – tumor MVD, and to determine the validity of DSCT in assessing angiogenic activity and neovascularity of HCC lesions.

Our study showed that the curve parameters generated from T-D curves of HCC lesions, such as PV and CER, were positively correlated to tumor MVD with statistical significance. As T-D curve parameters were representative of the hemodynamic characteristics of tumor microvasculature, this observation indicated that the degree of tumor enhancement on DSCT was affected by tumor MVD. The tumor enhancement degree could also truly reflect the distribution characteristics of tumor microvessels within a tumor mass, as the area with the greatest enhancement was often associated with the highest MVD. Higher tumor MVD was shown to be associated with worse degree of

malignancy and more potential of metastases[4,10], thus it is possible to estimate the biological behaviors of HCC in terms of aggressiveness and metastasis by calculating the parameters of HCC T-D curve through dynamic spiral CT scanning.

The patterns of T-D curves of HCC lesions also provided *in vivo* clues to the histomorphological distribution characteristics of tumor microvessels within a tumor mass. Type I curve was often histologically associated with rich blood sinusoids and microvessels in the interstitium, both demonstrating abundant positively stained tumor vascular endothelial cells. Such a histomorphological feature of microvessel-rich tumor interstitium might well explain the early rapid rise of the up-slope and the high amplitude of this type of T-D curves observed in this subset of HCC patients. As more and more contrast agents reached the sinusoids where the rate of blood flow was sluggish, alteration of the rise pace resulted in an abrupt turn of the curve up-slope configuration. Abundant, often dilated and tortuous sinusoids with positively stained tumor endothelial cells resulted in type II curve. Sluggish blood flow with prolonged accumulation of contrast agent in sinusoids might cause the slow and steady rise of the up-slope of T-D curve in this group of HCC patients. However, in 3 patients with type II curve, both sinusoids and interstitium showed rich positively stained endothelial cells. Two reasons might be implicated for this discrepancy between T-D curve pattern and histomorphological marker. First, the hemodynamic effect of rich blood sinusoids might overrun that of microvessel-rich interstitium in these 3 HCC patients, causing the distribution of contrast-containing blood within the tumor mass to be relatively slower. Misrepresentation due to sampling error was another possible reason. As the selected area of ROI was 1 cm, much larger than what could be represented on a histological slide, it was possible that the selected ROIs might actually contain many more sinusoids than what was shown on the corresponding histological slides in these 3 HCC patients. Type III curve was histologically characterized either by rich interstitium but with scanty interstitial microvessels and scanty blood sinusoids, or by rich sinusoids which were devoid of positively stained endothelial cells. These tumor sinusoids had structural and functional resemblance to those of normal liver sinusoids, therefore, the rise of the up-slope in this type of T-D curve was quite slow and flat in the hepatic arterial phase. In the patient with type III curve, both rich sinusoids and interstitial microvessels with positively stained endothelial cells were observed. We speculated that the cause might be the mismatch of selected ROI with the sampling site for histomorphological measurement, and the variation in tumor angiogenic activity within a tumor lesion, which could lead to the misrepresentation by MVD.

The study also found that the gross enhancement morphology of HCC lesions was related to the distribution of tumor microvessels within a tumor mass. As shown in Table 3, type A enhancement morphology was mainly seen in relatively small HCC lesions, while type C enhancement morphology was found in larger lesions. However, both types were histomorphologically characterized by rich blood sinusoids or coexistence of microvessel-rich interstitium, both of witch had abundant positively stained endothelial cells. Such findings might suggest that when a hypervascular HCC lesion was small, the distribution of tumor microvessels within it tended to be homogeneous, giving rise to the homogeneous enhancement appearance on DSCT scan. With the tumor became larger, intratumoral necrosis, fibrous septation and granulation formation occurred. The original homogeneity of tumor microvessels distribution was altered and distorted, so did the gross morphological enhancement patterns on CT images. Type B enhancement morphology showed that tumor interstitium was abundant in quantity, but either with scanty interstitial microvessels and few sinusoids, or with rich sinusoids that were devoid of positively stained endothelial cells. In sharp contrast, tumor microvessels with positively stained endothelial cells were rich in pseudocapsules of this type of HCC patients. Thus the gross morphological enhancement pattern could well reflect the underlying histomorphological characteristics of tumor microvessels in this group of HCC patients. Therefore, by analyzing the enhancement morphology of HCC lesions on dynamic spiral CT scan, it was possible to estimate both the *in vivo* tumor angiogenic activity and the distribution characteristics of tumor neovascularity. Compared to the measurement of histomorphological markers, dynamic spiral CT was able to maximally avoid the possibility of sampling errors and offered a comprehensive overview of the gross enhancement morphology of HCC lesions.

Our another interesting finding was that most of HCC lesions with intrahepatic metastases or daughter foci demonstrated characteristic hyperdense pseudocapsules on dynamic CT images corresponding to hepatic arterial phase. These pseudocapsules were histomorphologically characterized by very rich positively stained endothelial cells diffusely distributed in the connective tissues of pseudocapsules. Such an association indicated that hypervascularized tumor pseudocapsules with abundant interstitial structurally defective tumor microvessels[31] might facilitate intrahepatic metastasis or homogeneous spreading of HCC.

Though the close positive correlation of enhancement imaging features of HCC lesions revealed by DSCT with tumor MVD was demonstrated, several other factors, such as perfusion rate, microvessel permeability, and size or volume of extracellular space, might also influence the uptake rate of contrast agent by tumor tissue, thus affecting the configurations of T-D curve. Little has been known about major contributors for the difference in the contrast agent uptake rate[11,32]. We suspect that the differences might depend on the type or even subtype of tumors, and further studies are required to clarify this issue.

In conclusion, the characteristics of T-D curve of HCC revealed by DSCT scanning are closely related to tumor MVD. The grass enhancement morphology of HCC lesions on DSCT images can reflect the features of histomorphological distribution of tumor microvessels within a tumor. DSCT is valid for the *in vivo* assessment of tumor angiogenic activity and neovascularity of HCC lesions, which is very important in making differential diagnosis, evaluating tumor malignancy and aggressiveness, monitoring therapeutic effects, and determining the final outcome of HCC patients.

ACKNOWLEDGEMENT

Our thanks go to Dr. Luinan Yan, MD, and Dr. Sheng He, MD, for their valuable assistance of this research work.

REFERENCES

1 **Folkman J**, Shing Y. Angiogenesis. *J Biol Chem* 1992; **267**: 10931-10934

2 **Weidner N**, Semple J, Welch W, Folkman J. Tumor angiogenesis and metastasis: correlation in invasive breast carcinoma. *N Engl J Med* 1991; **324**: 1-8

3 **Weidner N**. Intratumor microvessel density as a prognostic factor in cancer. *Am J Pathol* 1995; **147**: 9-19

4 **Jinno K**, Tanimizu M, Hyodo I, Nishikawa Y, Hosokawa Y, Doi T, Endo H, Yamashita T, Okada Y. Circulating vascular endothelial growth factor (VEGF) is a possible tumor marker for metastasis in human hepatocellular carcinoma. *J Gastroenterol* 1998; **33**: 376-382

5 **Weidner N**, Carroll PR, Flax J, Blumenfeld W, Folkman J. Tumor angiogenesis correlates with metastasis in invasive prostate carcinoma. *Am J Pathol* 1993; **143**: 401-409

6 **Poon RT,** Ng IO, Lau C, Yu WC, Yang ZF, Fan ST, Wong J. Tumor microvessel density as a predictor of recurrence after resection of hepatocellular carcinoma: a prospective study. *J Clin Oncol* 2002; **20**: 1775-1785

7 **Augustin HG**. Antiangiogenic tumor therapy: will it work? *Trends Pharmacol Sci* 1998; **19**: 216-222

8 **Hama Y**, Shimizu T, Hosaka S, Sugenoya A, Usuda N. Therapeutic efficacy of the angiogenesis inhibitor O-(chloroacetylcarbamoyl) fumagillol (TNP-470; AGM-1470) for human anaplastic thyroid carcinoma in nude mice. *Exp Toxicol Pathol* 1997; **49**: 239-247

9 **Kin M,** Torimura T, Ueno T, Nakamura T, Ogata R, Sakamoto M, Tamaki S, Sata M. Angiogenesis inhibitor TNP-470 suppresses the progression of experimentally-induced hepatocellular carcinoma in rats. *Int J Oncol* 2000; **16**: 375-382

10 **Tomisaki S**, Ohno S, Ichiyoshi Y, Kuwano H, Maehara Y, Sugimachi K. Microvessel quantification and its possible relation with liver metastasis in colorectal cancer. *Cancer* 1996; **77**(8 Suppl): 1722-1728

11 **Hawighorst H**, Knapstein PG, Knopp MV, Vaupel P, van Kaick G. Cervical carcinoma: standard and pharmacokinetic analysis of time-intensity curves for assessment of tumor angiogenesis and patient survival. *MAGMA* 1999; **8**: 55-62

12 **Wild R,** Ramakrishnan S, Sedgewick J, Griffioen AW. Quantitative assessment of angiogenesis and tumor vessel architecture by computer-assisted digital image analysis: effects of VEGF-toxin conjugate on tumor microvessel density. *Microvasc Res* 2000; **59**: 368-376

13 **Sahin Akyar G**, Sumer H. Color Doppler ultrasound and spectral analysis of tumor vessels in the differential diagnosis of solid breast masses. *Invest Radiol* 1996; **31**: 72-79

14 **Raza S**, Baum JK. Solid breast lesions: evaluation with power Doppler US. *Radiology* 1997; **203**: 164-168

15 **Louvar E**, Littrup PJ, Goldstein A, Yu L, Sakr W, Grignon D. Correlation of color Doppler flow in the prostate with tissue microvascularity. *Cancer* 1998; **83**; 135-140

16 **Peters-Engl G**, Medl M, Mirau M, Wanner C, Bilgi S, Sevelda P, Obermair A. Color-coded and spectral Doppler flow in breast carcinoma-relationship with the tumor microvasculature. *Breast Cancer Res Treat* 1998; **47**: 83-89

17 **Stomper PC**, Winston JS, Herman S, Klippenstein DL, Arredondo MA, Blumenson LE. Angiogenesis and dynamic MR imaging gadolinium enhancement of malignant and benign breast lesions. *Breast Cancer Res Treat* 1997; **45**: 39-46

18 **Hawighorst H**, Knapstein PG, Weikel W, Knopp MV, Zuna I, Knof A, Brix G, Schaeffer U, Wilkens C, Schoenberg SO, Essig M, Vaupel P, van Kaick G. Angiogenesis of uterine cervical carcinoma: characterization by pharmacokinetic magnetic resonance parameters and histological microvessel density with correlation to lymphatic involvement. *Cancer Res* 1997; **57**: 4777-4786

19 **Pham CD**, Roberts TP, van Bruggen N, Melnyk O, Mann J, Ferrara N, Cohen RL, Brasch RC. Magnetic resonance imaging detects suppression of tumor vascular permeability after administration of antibody to vascular endothelial growth factor. *Cancer Invest* 1998; **16**: 225-230

20 **Hawighorst H**, Knapstein PG, Knopp MV, Weikel W, Brix G, Zuna I, Schonberg SO, Essig M, Vaupel P, van Kaick G. Uterine cervical carcinoma: comparison of standard and pharmacokinetic analysis of time-intensity curves for assessment of tumor angiogenesis and patient survival. *Cancer Res* 1998; **58**: 3598-3602

21 **Hawighorst H,** Schaeffer U, Knapstein PG, Knopp MV, Weikel W, Schonberg SO, Essig M, van Kaick G. Detection of angiogenesis-dependent parameters by functional MRI: correlation with histomorphology and evaluation of clinical relevance as prognostic factor using cervix carcinoma as an example. *Rofo Fortschr Geb Rontgenstr Neuen Bildgeb Verfahr* 1998; **169**: 499-504

22 **Hawighorst H,** Weikel W, Knapstein PG, Knopp MV, Zuna I, Schonberg SO, Vaupel P, van Kaick G. Angiogenic activity of cervical carcinoma: assessment by functional magnetic resonance imaging-based parameters and a histomorphological approach in correlation with disease outcome. *Clin Cancer Res* 1998; **4**: 2305-2312

23 **Mayr NA,** Hawighorst H, Yuh WT, Essig M, Magnotta VA, Knopp MV. MR microcirculation assessment in cervical cancer: correlations with histomorphological tumor markers and clinical outcome. *J Magn Reson Imaging* 1999; **10**: 267-276

24 **Miles KA,** Charnsangavej C, Lee FT, Fishman EK, Horton K, Lee TY. Application of CT in the investigation of angiogenesis in oncology. *Acad Radiol* 2000; **7**: 840-850

25 **Gossmann A,** Helbich TH, Mesiano S, Shames DM, Wendland MF, Roberts TP, Ferrara N, Jaffe RB, Brasch RC. Magnetic resonance imaging in an experimental model of human ovarian cancer demonstrating altered microvascular permeability after inhibition of vascular endothelial growth factor. *Am J Obstet Gynecol* 2000; **183**: 956-963

26 **Okuhata Y,** Brasch RC, Pham CD, Daldrup H, Wendland MF, Shames DM, Roberts TP. Tumor blood volume assays using contrast-enhanced magnetic resonance imaging: regional heterogeneity and postmortem artifacts. *J Magn Reson Imaging* 1999; **9**: 685-690

27 **Padhani AR,** Neeman M. Challenges for imaging angiogenesis. *Br J Radiol* 2001; **74**: 886-890

28 **Roberts HC,** Roberts TP, Brasch RC, Dillon WP. Quantitative measurement of microvascular permeability in human brain tumors achieved using dynamic contrast-enhanced MR imaging: correlation with histologic grade. *Am J Neuroradiol* 2000; **21**: 891-899

29 **Miles KA.** Tumour angiogenesis and its relation to contrast enhancement on computed tomography: a review. *Eur J Radiol* 1999; **30**: 198-205

30 **Kwak BK,** Shim HJ, Park ES, Kim SA, Choi D, Lim HK, Park CK, Chung JW, Park JH. Hepatocellular carcinoma: correlation between vascular endothelial growth factor level and degree of enhancement by multiphase contrast-enhanced computed tomography. *Invest Radiol* 2001; **36**: 487-492

31 **Less JR**, Skalak TC, Sevick EM, Jain RK. Microvascular architecture in a mammary carcinoma: branching patterns and vessel dimensions. *Cancer Res* 1991; **51**: 265-273

32 **Degani H**, Gusis V, Weinstein D, Fields S, Strano S. Mapping pathophysiological features of breast tumors by MRI at high spatial resolution. *Nat Med* 1997; **3**: 780-782

Edited by Ren SY and Wang XL